# 1
# Introduction

## 1.1 The fact of turbulent flow

Man has evolved within a world where air and water are, by far, the most common fluids encountered. The scales of the environment around him and of the machines and structures his ingenuity has created mean that, given their relatively low kinematic viscosities, the relevant global Reynolds number, Re, associated with the motion of both fluids is, in most cases, sufficiently high that the resultant flow is of the continually time-varying, spatially irregular kind we call *turbulent*.

If, however, our Reynolds number is chosen not by the overall physical dimension of the body of interest – an aircraft wing, say – and the fluid velocity past it but by the smallest distance over which the velocity found within a turbulent eddy changes appreciably and the time over which such a velocity change will occur, its value then turns out to be of order unity. Indeed, one might observe that if this last Reynolds number, traditionally called the micro-scale Reynolds number, $\mathrm{Re}_\eta$, were significantly greater than unity, the rate at which the turbulent kinetic energy is destroyed by viscous dissipation could not balance the overall rate at which turbulence 'captures' kinetic energy from the mean flow.

This immutable fact of turbulence life lies at the heart of the problem of computing turbulent flows. Any complete numerical solution of the Navier–Stokes equations must resolve accurately these fine-scale motions as well as the large-scale overall flow picture in which we are interested. Because of the range of scales to be resolved, from the fine-scale dissipative motions to the complete flow field, it is only feasible at present to carry out such a *direct numerical simulation* (DNS) of turbulent flow for relatively simple shear flows for overall Reynolds numbers typically of order $10^5$ and then only with 'supercomputer' scales of hardware. If one is, thus, to embark on the computation of practically interesting turbulent flows reasonably cheaply (recognizing that in most cases one needs to make tens or even hundreds of computations of the same geometric configuration to obtain

a sufficiently full picture), some form of modelling is essential to compensate for being unable to resolve directly all the turbulence scales as well as the mean flow.

## 1.2 Broad options in modelling

Two broad strategies for modelling are commonly employed.

- Large-eddy simulation (LES), where one resolves as large a proportion of the turbulent fluctuations as one judges necessary (or can afford) and applies a model – a sub-grid-scale (sgs) model – to account for the effects of those motions of a finer scale than can be resolved with the adopted mesh. The principal needs, so far as the dynamic field is concerned, are to account for momentum transfer by the unresolved motions and to ensure that kinetic energy is removed from the simulation at the appropriate rate (which amounts to modelling the effective sgs stresses created in the fluid).
- Reynolds-averaged Navier–Stokes (RANS) equations, in which the effects of *all* the turbulent fluctuations are subsumed within the model – generally termed *the turbulence model*. As with LES, the non-linearity of the convective transport means that models are needed to account for the effective turbulent fluxes of momentum, enthalpy and chemical species in their respective transport equations. These are termed the turbulent (or Reynolds) stresses and the turbulent heat or mass fluxes; they emerge naturally in Chapter 2 and are shown symbolically as $\overline{u_i u_j}$ and $\overline{\theta u_j}$, where $u_i$ and $\theta$ denote turbulent fluctuations of velocity and the scalar in question about their mean value and the overbar implies time averaging.

It is this second approach to modelling turbulence that is the principal focus of the present book. There are also strategies that are, effectively, a blend of these two approaches. Such schemes form the subject of the book's final chapter; but, for the present, they are not considered further, except to remark that the development of such hybrid approaches reflects, in part, the inadequacies of the RANS models that are most commonly used in engineering computations. Thus, if more generally applicable approaches to RANS closure are adopted, that, on the one hand, reduces the need to resort to such hybrid LES-RANS schemes while, on the other, also provides a more secure RANS component in situations where such combined approaches are necessary or desirable.

A comparative illustration of the numerical resolution of turbulent flow in a pipe or channel required by these different numerical approaches – DNS, LES and RANS – is shown in Fig. 1.1. A random-like oscillating signal with sharp peaks (top figure, left) provides a snapshot of the true instantaneous velocity, $\hat{U}$, in a vertical cross plane. A properly resolved DNS (with the computational cells

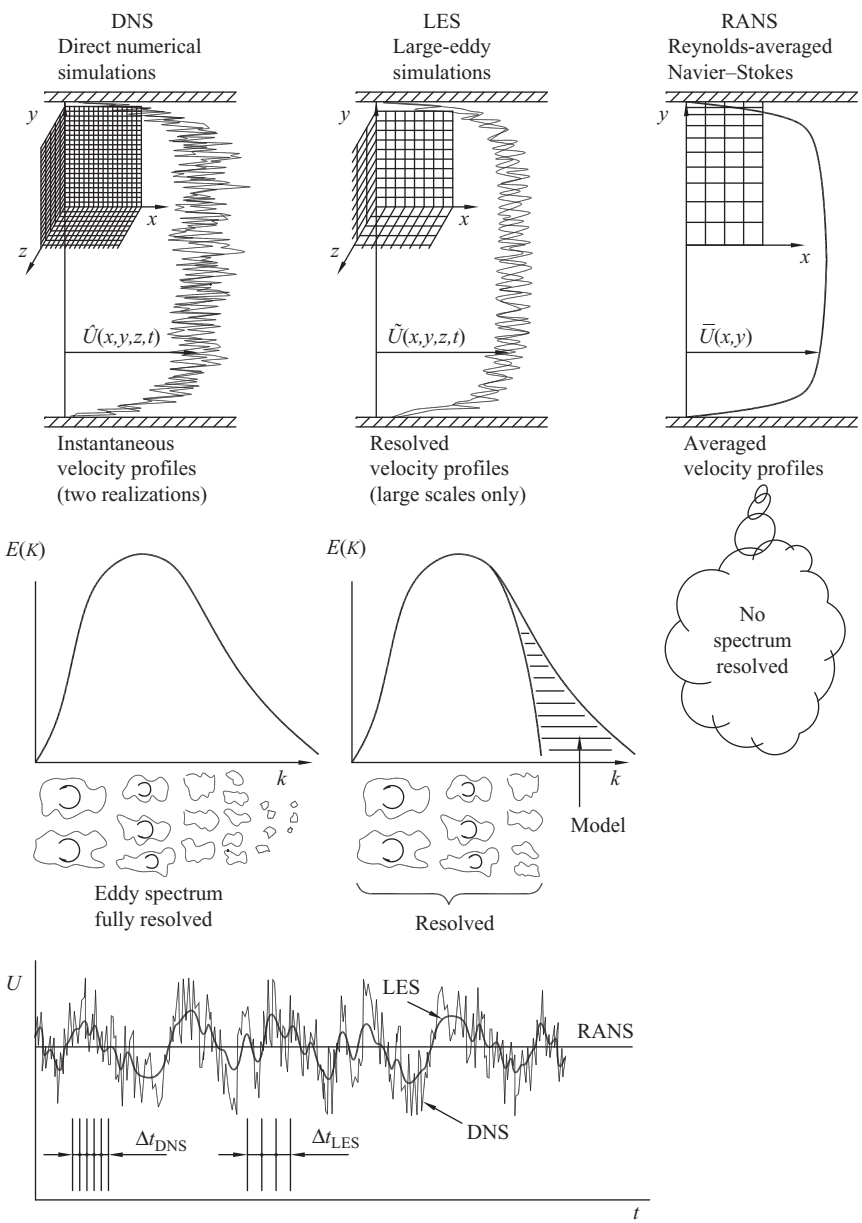


Fig. 1.1 Illustrative comparison of DNS, LES and RANS simulations of a fully developed, steady turbulent flow in a pipe or a plane channel. Top: typical computational grids and sketches of a set of instantaneous velocity profiles ($\hat{U}$) from DNS, filtered velocity profiles ($\tilde{U}$) from LES, and the time-averaged profile ($\bar{U}$) obtained by RANS. Centre: a sketch of the resolved energy spectrum $E(\kappa)$ for DNS and LES (note: RANS is also called 'one-point closure' because it computes the averaged turbulence properties at a point in space with no information on the turbulence spectrum). Bottom: time signal at a point in the flow and typical time steps for DNS and LES. The RANS solution, by definition, gives a constant velocity at a point in a steady flow.

smaller than the smallest important eddy size) will provide the complete range of wavelengths of velocity fluctuations. The instantaneous velocity profile obtained by LES (top figure, middle) also shows a range of wavelengths, but because the computational mesh is coarser, the signal is somewhat smoother, representing the filtered velocity $\tilde{U}$. High frequencies, i.e. those with a wavelength smaller than the computational cells, are absent because they have been filtered out. The top-right figure shows the time-averaged velocity $\bar{U}$ which exhibits a smooth profile that can be obtained with a much coarser grid and which, for a simple shear flow such as considered here, may be just two dimensional.

The second row of figures illustrates the *resolved* energy spectrum $E(\kappa)$ determined using each of the methods. Here $E(\kappa)$ represents the contribution to the turbulence kinetic energy from all Fourier modes in the range from $\kappa$ to $\kappa + d\kappa$, where $\kappa = 2\pi/\lambda$ is the wavenumber modulus and $\lambda$ is the wavelength. Naturally, DNS should provide the complete spectrum, while LES excludes only the high wavenumber portion (beyond $\kappa_c = 2\pi/\Delta$, where $\Delta$ is the characteristic mesh size). In contrast, RANS can provide *no information* about the turbulence spectrum, but simply the value of the turbulence energy that would be obtained by integrating over the whole wavenumber range for any point in space.

The bottom figure illustrates the three methods in a different way: here a time record of fluid velocity is shown at a point in space in a steady flow. Again, the strongly oscillating peaky signal (such as would be recorded by a hot-wire anemometer) is representative of a typical DNS of velocity fluctuations at a point. The smoother oscillating signal is a typical LES result, whereas the RANS record would simply give a constant value. Resolving the DNS signal requires very small time steps, whereas LES tolerates a somewhat larger time step corresponding with the coarser computational mesh.

Both LES and RANS have particular strengths and dedicated proponents. Because, using LES, with the numerical solver one resolves directly a large proportion of the energy-containing turbulent motions, the model is less crucial to the computed behaviour of the flow than it is with RANS. Thus, a far from accurate sgs model may nevertheless lead to satisfactory numerical simulations. Just how important the sgs model is naturally depends on how large a proportion of the total effect of the turbulence it is required to carry. Currently, the most common strategy in sgs modelling is to assume that the magnitude of the components of the sgs stresses is directly proportional to the corresponding components of the resolved strain, the coefficient of proportionality being what is termed the sgs kinematic viscosity. The computational cost of an LES calculation naturally depends greatly on the fineness of the computational mesh chosen.

With a RANS approach, to a far greater extent than with LES, the fidelity of the computed flow hinges on a wise choice of model. The great majority of computations at present, particularly those for industrial applications for

complex-shaped configurations, still employ a linear eddy-viscosity model where the local value of the turbulent (or eddy) kinematic viscosity, $\upsilon_t$, is computed in the course of the solution, usually by way of supplementary transport equations for what amount to representative length and time scales for the energy-containing turbulent motions.

Within RANS there is, however, a hierarchy of alternative, more elaborate modelling strategies available, ranging from non-isotropic turbulent viscosity models to schemes which provide modelled transport equations of the individual turbulent stresses (or second moments) as well as their diffusion (the third moments). The focus of this book is on such alternative strategies with our primary attention being on modelling the second moments. The reason for this choice is simply that turbulent shear flows are not in any general sense describable by a model based on a linear eddy-viscosity model, while a well-crafted second-moment closure extends greatly the range of flows and phenomena that can be captured. Merely considering the stress-generation processes, as is done briefly in Section 1.3, allows one to appreciate why turbulent flows respond, qualitatively, as they do to the application of mean flow deformations of various types.

The discussion on modelling via second-moment closure has so far considered simply the turbulent stresses. If the processes of interest involve heat or mass transport, the averaged forms of the thermal energy and species transport equations likewise contain unknown turbulent second-moment correlations: the turbulent heat and species fluxes. Within a linear eddy-viscosity scheme these rates of transfer in any direction are taken directly proportional to the corresponding spatial gradient of mean temperature and mean species concentration, respectively. Such an assumption has similar shortcomings to that of the eddy viscosity approximation for momentum transport. Solving transport equations for these other second moments brings corresponding benefits to those for the turbulent stresses, especially where buoyant force fields are significant.

## 1.3 A preview of the mean-strain generation processes in the stress-transport equation

One of the attractions of second-moment closure compared with simpler approaches to modelling is that the second-moment generation terms are exactly represented and thus require no further approximation. This fact means that, where these terms are major contributors to the budget for the second moment in question, one is half-way to closure without having to make any approximations. Moreover, without completing a model for the remaining processes, one can often infer the character of a turbulent flow just by simply noting how the generation

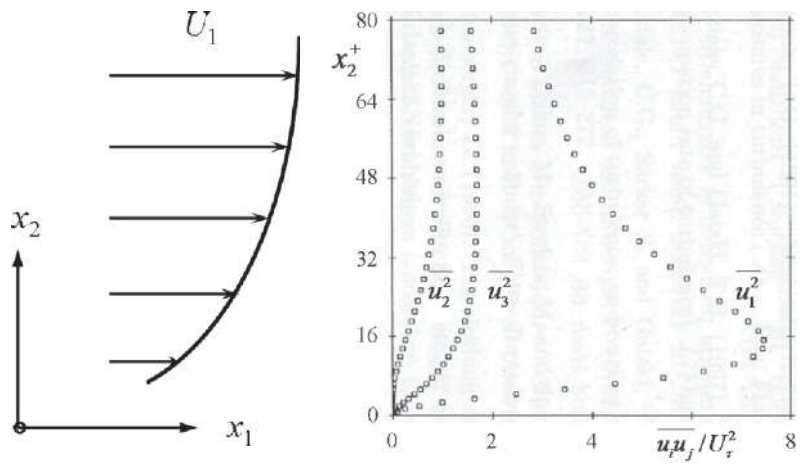


(a) (b)

Fig. 1.2 A simple shear flow: (a) typical mean velocity profile; (b) turbulent normal stress components in a plane channel flow, as a function of the non-dimensional wall distance $x_2^+ \equiv x_2 U_\tau/\nu$ (where $U_\tau$ is the wall friction velocity and $\nu$ is fluid kinematic viscosity). From the DNS of Kim *et al.* (1987).

is distributed among the turbulent stresses or heat fluxes for different externally applied conditions.

A formal derivation of the second-moment equations is deferred to Chapter 2 but here, to convey in advance some impression of the insight gained from a knowledge of the mean-strain generation process, we examine a few examples for commonly arising strain fields. In the absence of force fields, the interaction between the mean strain and the existing turbulence provides the source for further stress creation. Thus, in most circumstances, once a flow becomes turbulent it remains turbulent. The turbulent stress-generation tensor, $\mathcal{P}_{ij}$, in a uniform density flow will be shown in §2.3 to be given by

$$\mathcal{P}_{ij} = -\left(\overline{u_i u_k}\frac{\partial U_j}{\partial x_k} + \overline{u_j u_k}\frac{\partial U_i}{\partial x_k}\right) \tag{1.1}$$

where $\overline{u_i u_j}$ denotes the turbulent stress and $\partial U_i/\partial x_k$ is the gradient of the mean-velocity component in direction $x_k$.

Let us first see how these generation terms are distributed among the different Reynolds-stress components for the case of a simple shear flow where the mean flow is purely in direction $x_1$ and varies only in the $x_2$ direction, Fig. 1.2a. This is very nearly the situation that applies in a two-dimensional boundary layer. The resultant values of $\mathcal{P}_{ij}$ for each of the six stress components are obtained by assigning appropriate values to $i$ and $j$. The repeated subscript $k$ signals that elements carrying that subscript are to be summed with $k$ taking successively the values 1, 2

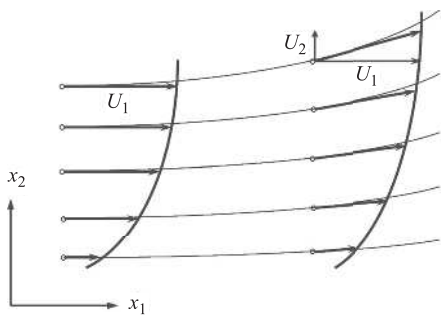


Fig. 1.3 Example of a mildly curved turbulent shear flow.

and 3. In the present case, however, the mean velocity varies only in direction $x_2$, so only $k = 2$ makes a contribution to $\mathcal{P}_{ij}$. The reader may thus readily verify that:

$$\begin{aligned}
\overline{u_1^2} \quad & \mathcal{P}_{11} = -2\,\overline{u_1 u_2}\frac{\partial U_1}{\partial x_2} \\
\overline{u_2^2} \quad & \mathcal{P}_{22} = 0 \\
\overline{u_3^3} \quad & \mathcal{P}_{33} = 0 \\
\overline{u_1 u_3} \quad & \mathcal{P}_{13} = 0 \\
\overline{u_2 u_3} \quad & \mathcal{P}_{23} = 0 \\
\overline{u_1 u_2} \quad & \mathcal{P}_{12} = -\overline{u_2^2}\frac{\partial U_1}{\partial x_2}.
\end{aligned} \tag{1.2}$$

It is noted from the last of these results that the generation rate of the shear stress, $\overline{u_1 u_2}$, is opposite in sign from the mean velocity gradient, a fact which explains why the shear stress itself normally has a sign opposite from the velocity gradient. Note, too, that turbulent velocity fluctuations in the direction of the mean velocity gradient are instrumental in creating that shear stress (or momentum transfer). Regarding the normal stresses, it is perhaps surprising that the only component in which there is a generation is the streamwise component, $\overline{u_1^2}$. As reference to thin shear flow data readily confirms, Fig. 1.2b, this component is by far the largest stress though turbulent fluctuations do occur in all directions. Where, in practice, the source of the fluctuating energy (or normal stresses) in directions $x_2$ and $x_3$ comes from will become clear in Chapter 2.

Let us next add a small degree of complexity to the strain field by imagining a weak streamline curvature in the $x_1$–$x_2$ plane, Fig. 1.3. We retain Cartesian coordinates so the curvature manifests itself by a non-zero value of $\partial U_2/\partial x_1$. Thus, from Eq. (1.1) the shear-stress generation becomes:

$$\mathcal{P}_{12} = -\left(\overline{u_2^2}\frac{\partial U_1}{\partial x_2} + \overline{u_1^2}\frac{\partial U_2}{\partial x_1}\right). \tag{1.3}$$

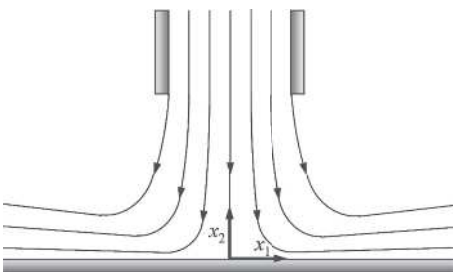


Fig. 1.4 Sketch of the stagnation region in a jet impinging normally on a flat wall.

It is evident from Fig. 1.2b that even far from the wall $\overline{u_1^2}$ is at least twice as large as $\overline{u_2^2}$, a situation that also pertains in strong free shear flows, like a jet. In a flow past a solid surface, however, as one progressively approaches the wall, the disparity between the two normal stresses becomes progressively greater, Fig. 1.2b. Thus, the effect of the curvature term in Eq. (1.3) becomes greatly amplified. Indeed, the great sensitivity of boundary layers to wall curvature has been known for many years (Bradshaw, 1973). If, however, one were to assume turbulent stresses were represented by an isotropic turbulent viscosity, $\nu_t$, one would conclude:

$$\overline{u_1 u_2} = -\nu_t \left( \frac{\partial U_1}{\partial x_2} + \frac{\partial U_2}{\partial x_1} \right). \tag{1.4}$$

In this representation, the weighting of the two strain components is equal, each being multiplied by the scalar turbulent viscosity.[1] The above example provides the first illustration of the over-simplification produced by the eddy viscosity formula alluded to in §1.2.

An even sharper example is provided in the case of impinging flow. Let us consider the rate at which turbulent kinetic energy is being produced by virtue of the mean-flow straining along the centre-line of a plane, symmetric stagnation flow, Fig. 1.4. The turbulence energy, $k$, is just half the sum of the normal stresses and its production rate, $\mathcal{P}_k$, is thus:

$$\mathcal{P}_k = -\overline{u_i u_j} \frac{\partial U_i}{\partial x_j}. \tag{1.5}$$

Along the symmetry plane the turbulence energy generation arises purely from the normal strains, which, we assume, are adequately represented by the potential flow solution for plane stagnation flow: $\partial U_1/\partial x_1 = -\partial U_2/\partial x_2 = C$, a constant.

[1] It should be recognized that Eq. (1.3) expresses the *production rate* of the shear stress, while Eq. (1.4) refers to the shear stress itself. However, as will be seen later, at least in stress components with major stress generation terms, the stress production rate is indeed closely related to the magnitude of the stress.

Thus:

$$\mathcal{P}_k = -\left(\overline{u_1^2}\frac{\partial U_1}{\partial x_1} + \overline{u_2^2}\frac{\partial U_2}{\partial x_2}\right) = C\left(\overline{u_2^2} - \overline{u_1^2}\right). \tag{1.6}$$

From Eq. (1.6) it is evident that for this flow the rate of production of turbulent kinetic energy depends on the difference between the normal stresses, i.e. on the anisotropy of the turbulent stress field. The value of $\mathcal{P}_k$ may be positive, negative or zero depending on the relative levels of the two normal stresses. If, however, the turbulence energy generation had been represented by a turbulent viscosity, it is easily verified that the following form would be obtained:

$$\mathcal{P}_k = 4\nu_t C^2. \tag{1.7}$$

Equation (1.7) implies no such sensitivity to anisotropy; indeed, in all circumstances it returns an erroneously high energy generation rate. Computations of impinging flows with eddy viscosity models thus lead to quite spurious peaks of turbulence energy in the vicinity of a stagnation point unless problem-specific corrections are adopted (Taulbee and Tran, 1988; Craft *et al.*, 1993; Durbin, 1996). A similar anomalous outcome of using eddy-viscosity models has also been observed in other flows where normal straining plays an important role. For example, both the analytical and numerical solutions for confined homogeneous turbulence subjected to cyclic compressive/dilatational strain show that depending on the sign of the strain the turbulence production takes alternately positive and negative values, resulting in zero net production over a cycle (Hadžić *et al.*, 2001). Because of the continuous dissipation, however, both the turbulent kinetic energy and the characteristic turbulence frequency (the reciprocal of the turbulent time scale) eventually decay, irrespective of the initial turbulence level, anisotropy of the stress field or Reynolds number. In contrast, eddy viscosity models predict an erroneous continual increase of the turbulent kinetic energy because of the incorrect positive generation of turbulence during the compression phase. Other examples where the broad character of a turbulent flow can be inferred from considering the stress generation terms may be found in flows affected by body forces whether due to system rotation (Coriolis force), density stratification (buoyant force) or magnetic field (Lorentz force). Such cases are discussed in detail in §4.5.

## 1.4 Some consequences of the no-slip boundary condition at a wall

At a rigid, stationary wall the velocity goes to zero, at least in the continuum regime to which attention is limited. This condition applies to the turbulent fluctuations as well as to the mean velocity. Thus the turbulent stresses all vanish at the wall and wall friction is exerted through purely viscous effects just as in laminar flow.

As is evident from Fig. 1.2b, however, the turbulent velocity components do not all increase at the same rate as one moves away from the wall. There are several reasons for this, as will emerge in Chapters 4 and 6, but one that is examined here briefly is the constraint applied by mass conservation. For a uniform density flow, as will be shown formally in §2.3, the turbulent velocity fluctuations as well as the mean flow are divergence free:

$$\frac{\partial u_1}{\partial x_1} + \frac{\partial u_2}{\partial x_2} + \frac{\partial u_3}{\partial x_3} = 0. \tag{1.8}$$

This equation applies everywhere, including the fluid–wall interface $x_2 = 0$. But on this surface $\partial u_1/\partial x_1 = \partial u_3/\partial x_3 = 0$ since $u_1$ and $u_3$ are zero throughout the $x_1 \sim x_3$ plane. It follows that $\partial u_2/\partial x_2$ must also be identically zero there. Thus, we deduce that, while the root-mean-square values of $u_1$ and $u_3$ initially increase linearly with distance from the wall, $x_2$, the corresponding value of $u_2$ can only increase as $x_2^2$, while the shear stress $\overline{u_1 u_2}$ can at most increase as $x_2^3$. These inferred exponents of the different stress-component variations will be seen in Chapter 6 to be fully in accord with DNS data.

The fact that $\overline{u_1 u_2}$ increases as the cube of the distance from the wall implies that initially, for small $x_2$, this turbulent shear stress will be negligible compared with viscous shear stress. As one proceeds further from the wall, however, one enters a region where there is a rapid changeover to a regime where the turbulent stress becomes the dominant contributor to momentum transfer. Since the total shear stress (viscous plus turbulent) is very nearly constant over what is a very thin layer (compared with the shear flow as a whole), there will inevitably be a rapid reduction in the slope of the mean velocity. That is, one moves from a region where viscous action ($\nu \partial U_1/\partial x_2$) is the principal mechanism for momentum transfer to one where most of the momentum transport is by turbulence. This rapid changeover is clearly evident from the mean velocity profiles in Fig. 1.1, top right (denoted as RANS), and in more detail in Fig. 6.1.

In fact, in a simple shear flow, the maximum generation rate of turbulent kinetic energy occurs right in this changeover region. For, this will occur where

$$\frac{d}{dx_2}\left(\overline{u_1 u_2}\frac{dU_1}{dx_2}\right) = 0, \tag{1.9}$$

or, on expanding the differential, where:

$$\overline{u_1 u_2}\frac{d^2 U_1}{dx_2^2} + \frac{dU_1}{dx_2}\frac{d\,\overline{u_1 u_2}}{dx_2} = 0. \tag{1.10}$$

On the assumption that the total shear stress ($(\nu dU_1/dx_2) - \overline{u_1 u_2}$) is changing much less rapidly than its constituent parts, we can replace the turbulent shear-stress derivative in Eq. (1.10) by the corresponding derivative of viscous stress. With this